

The thermal structure of a wind-driven Reynolds ridge

Supathorn Phongikaroon, K. Peter Judd, Geoffrey B. Smith, Robert A. Handler

Abstract In this study, we investigate the nature of a Reynolds ridge formed by wind shear. We have simultaneously imaged the water surface, with a deposit of a monolayer of the surfactant, oleyl alcohol, subject to different wind shears, by using a high-resolution infrared (IR) detector and a high-speed (HS) digital camera. The results reveal that the regions around the wind-driven Reynolds ridge, which have subtle manifestations in visual imagery, possess surprisingly complex hydrodynamical and thermal structures when observed in the infrared. The IR measurements reveal a warm, clean region upstream of the ridge, which is composed of the so called *fishscale* structures observed in earlier investigations. The region downstream of the ridge is composed of colder fluid which forms two counter-rotating cells. A region of intermediate temperature, which we call the mixing (wake) region, forms immediately downstream of the ridge near the channel centerline. By measuring the velocity of the advected *fishscales*, we have determined a surface drift speed of about 2% of the wind speed. The spanwise length-scale of the structures has also been used to estimate the wind shear. In addition, a comparison of IR and visual imagery shows that the thermal field is a very sensitive indicator of the exact position of the ridge itself.

1 Introduction

The surfaces of natural bodies of water, such as lakes, streams, and oceans, are typically contaminated with thin films of surface active agents, or surfactants. The presence or absence of these surfactants is of importance in many diverse fields, including oceanography and remote sensing. These films are frequently found to be stretched and

compressed by water currents, wind forcing, and other processes. When the forcing is sufficiently strong, a portion of the water surface may actually be cleaned of surfactant. Under these circumstances, a thin line of demarcation can be observed between the contaminated and uncontaminated regions. It has been found that this line is, in reality, a slightly elevated region of the surface, and has become known as a Reynolds ridge (Reynolds 1900; Langton 1872; Edser 1926; Satterly and Turnbull 1929; McCutchen 1970).

The first report of the visual appearance of a line of demarcation between a surfactant contaminated region and an uncontaminated region was that of Franklin et al. (1774). Much later, Reynolds (1900) showed that surface tension gradients were critical in understanding the origin of the line, which is formed as a result of the surface contaminant being trapped against a barrier by an oncoming stream. More recently, theoretical models have been developed (McCutchen 1970; Harper and Dixon 1974) based on boundary layer theory, which attempt to predict the shape and size of the ridge. These theories were largely confirmed by recent experimental studies in which Schlieren methods (Sellin 1968) or specular reflection-based methods (Scott 1982) were used to measure the surface slopes in the region of the ridge. Other recent experiments (Warncke et al. 1996; Vogel et al. 2001) have employed advanced imaging and digital particle image velocimetry (DPIV) techniques to further explore the details of the hydrodynamics beneath the ridge.

The investigations described above were principally devoted to the relatively simple case in which a Reynolds ridge is formed by water flow compressing a surface film against a barrier. In the present work, we investigate the more complex case in which wind shear drives the flow. We suspect that this is a relatively common situation in natural environments, where surface slicks are formed on bodies of water due to the compression of surfactant material by the wind (Woodcock 1941; Scott 1972; Romano 1996). Our goal is to elucidate the formation and dynamics of the wind-driven Reynolds ridge. Imagery of the free surface flow in the vicinity of the ridge was captured simultaneously using an infrared (IR) detector and a high-speed (HS) digital camera. We show below that high-resolution IR methods are effective in elucidating the complex fluid physics in the vicinity of the Reynolds ridge. In particular, by comparing IR imagery with HS digital imagery, we conclude that IR methods can be used to accurately locate the position of the ridge.

Received: 12 August 2003 / Accepted: 25 January 2004
Published online: 19 March 2004
© Springer-Verlag 2004

S. Phongikaroon (✉), K. Peter Judd, G. B. Smith, R. A. Handler
Remote Sensing Division, Naval Research Laboratory, Washington,
DC20375, USA
E-mail: supathorn@nrl.navy.mil

We thank Professor K.A. Flack at the United States Naval Academy for lending us the wind tunnel. We also want to thank Dr. C. Trump for help in constructing the wind-wave tunnel. This work is supported by the National Research Council through the Naval Research Laboratory, and the Office of Naval Research.

2 Experimental setup and method

In our laboratory experiments, a wind-driven Reynolds ridge was generated by exposing the free surface of a small tank of water to an air flow generated by a wind tunnel (Fig. 1). A stationary tank manufactured from Plexiglas is inserted between the inlet and outlet sections of a wind tunnel. The downstream end of the channel is dammed to simulate a shoreline. The length and width of the channel are $L=35.0$ cm and $W=10.4$ cm, respectively. To reduce the presence of natural surfactants, the tank was filled with doubly distilled water and was overflowed for half an hour prior to each experimental run. The water level was then adjusted to a height of approximately 1 mm below the top of the sluice ($H=10.3$ cm). The wind speed through the tunnel was measured using a commercial pressure transducer (MKS Baratron 223B) connected to a pitot tube. A long entrance length region (30.5 cm) from the plenum to the edge of water allows a well developed, air-side turbulent boundary layer to form. This turbulence develops sufficient surface shear to compress the contaminated film, as shown in Fig. 1. Imagery of the free surface flow in the vicinity of the ridge was captured simultaneously using an IR camera (an Indigo CCD camera having a 320×256 array) and an HS digital camera (Kodak Ektaprop Model 4540 with a 256×256 array).

The IR imagery was obtained by looking down through a silicone IR window (20.3 cm \times 13.0 cm \times 0.64 cm), which allowed the transmission of radiation in the 3–5 μ m wavelength range. In this wavelength band, the mean optical depth in the water is approximately 20 μ m, so we may interpret the IR imagery, for all practical purposes, as a map of the surface temperature field. The IR camera, with a thermal resolution of ± 0.02 K, is particularly well suited to capture the small temperature gradients in the vicinity of the ridge. The HS digital imagery was captured from the bottom of the facility, looking up through a Plexiglas panel.

Oleyl alcohol was used as the surfactant for this experiment. A partial volume of prepared stock solution

was withdrawn and mixed with silver-coated polystyrene particles obtained from Dantec (specific gravity near unity) to aid the detection of the Reynolds ridge with the HS digital camera. It should be mentioned that the addition of the silver-coated particles does not affect the thermal structure obtained from the IR camera. A micro-syringe was used to deposit a 4- μ L drop of this mixture onto the free surface. The spreading drop left an oleyl alcohol monolayer covering the entire free surface. The final concentration of oleyl alcohol in our experiments, before compression of the film by the wind, was 0.03 μ g/cm 2 .

3 Results

A sequence of IR images depicting the temporal evolution of the Reynolds ridge subsequent to the application of wind stress is shown in Fig. 2. These images were selected from a sequence of images obtained at a sampling rate of 30 frames per second. Each IR image represents a 10.4 cm \times 12.8 cm region. The top of these images is 6.1 cm downstream from the leading edge of the channel. Although we have performed experiments over a range of wind speeds from 2 m/s to 9 m/s, we show here a typical case with a mean wind speed of 7.8 m/s (from top to bottom). The tunnel inlet temperature and relative humidity were 24.5°C and 36%, respectively, with these conditions remaining constant throughout all experiments. The grayscale is an indication of the surface temperature, going from warm to cold as the scale goes from light to dark. The temperature difference between these two extreme regions is approximately 1.0°C. A thermal front first appears at the top of Fig. 2b, and becomes much clearer in Fig. 2c. We show below that this front does in fact coincide with the Reynolds ridge and it is, therefore, designated as such in the figure. There are several streamwise streaks (lighter regions) which are most prominent in Fig. 2b. We expect that these streaks may be signatures of Langmuir circulation (Woodcock 1941; Langmuir 1938; Leibovich 1983). However, further work would be necessary to confirm our conjecture. We note

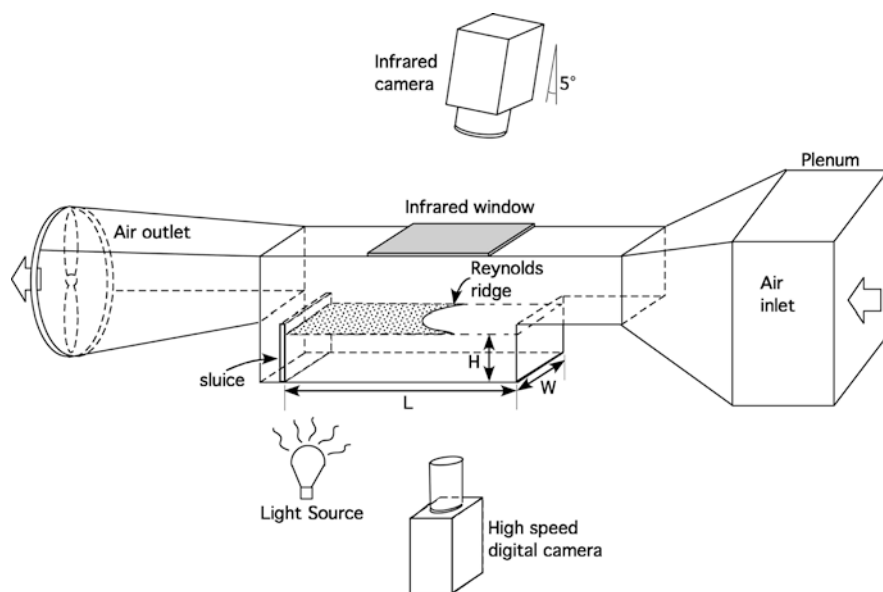


Fig. 1. The experimental setup of a wind-wave tunnel. The shaded region behind the ridge represents a compressed surfactant film. The length, width, and height are $L=35.0$ cm, $W=10.4$ cm, and $H=10.3$ cm, respectively. Note: not drawn to scale

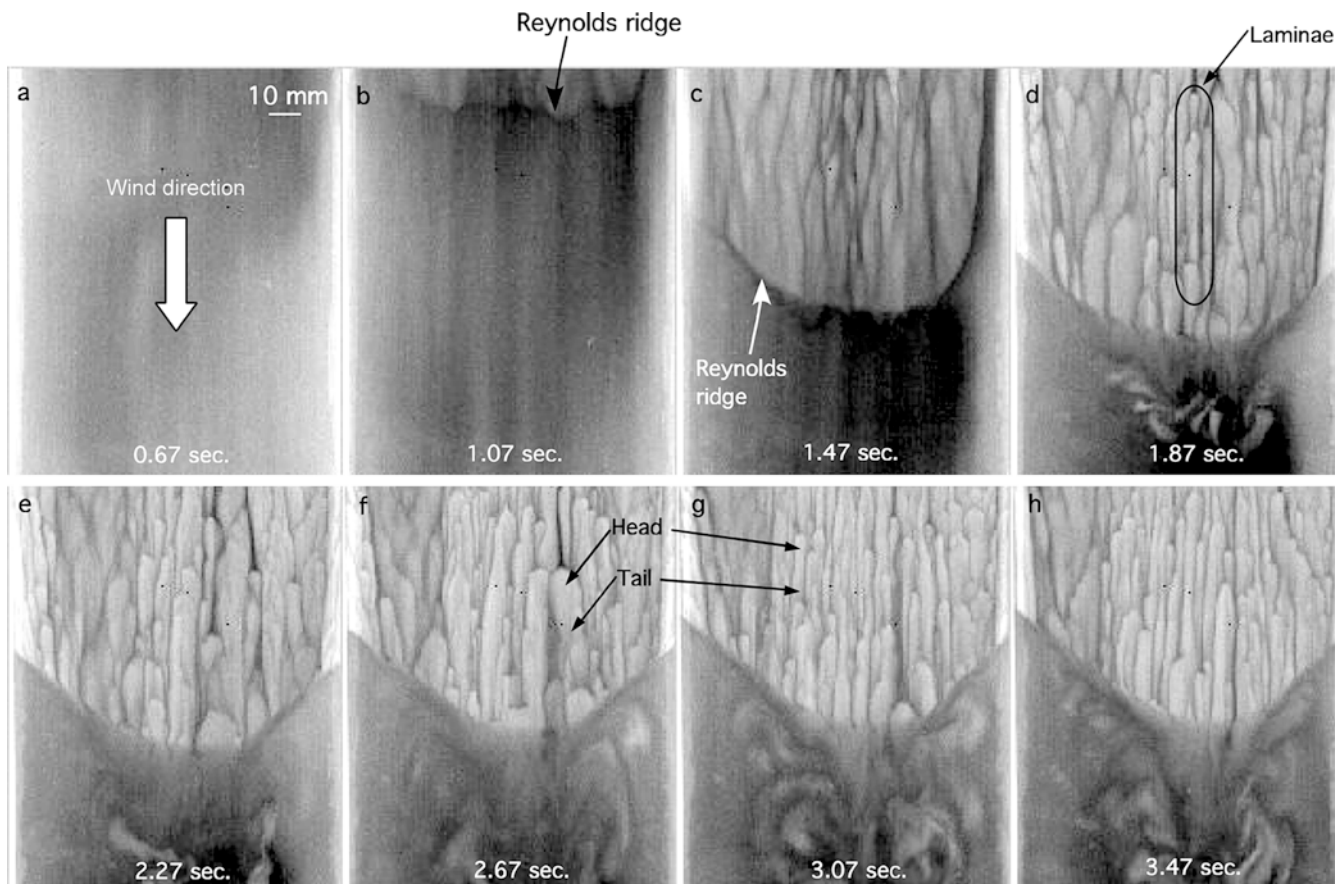


Fig. 2a-h. A time sequence of IR images showing the formation of a Reynolds ridge. The Reynolds ridge is first visible in b, and is quickly pushed downstream by the wind to a point closest to the downstream gate, seen in d. The ridge then rebounds, and attains

its steady state position, seen in g. In b and c, there are streamwise streaks, as mentioned briefly in the text, appearing behind the ridge. Both g and h show two recirculation regions behind the ridge

that such streamwise instabilities have been observed previously in IR imagery (Smith et al. 1998; Veron and Melville 2001). The furthest downstream location of the ridge appears in Fig. 2e, and is followed by a slight upstream rebound. Ultimately, the Reynolds ridge reaches its final equilibrium position, where it can be maintained indefinitely, as long as the applied wind shear and surfactant concentration remain constant (Fig. 2h). Generally, at low wind speed (<5 m/s), a Reynolds ridge forms rapidly and reaches an equilibrium position (steady state) after approximately 6 s.

We observe (Fig. 2d) that the warm region, which has been swept clean of surfactant, is composed of an array of streamwise-oriented laminae. These laminae, which have been described in detail elsewhere (Handler et al. 2001), are caused by the shearing of rising buoyant plumes. The laminae, which have been termed *fishscales*, have a characteristic head-tail structure, as indicated in Fig 2f, g. It was found, by Handler et al. (2001), that the characteristic cross-stream length-scale associated with the laminae was $100\nu/u^*$, where ν is the kinematic viscosity of water, $u^*=(\tau/\rho)^{1/2}$ is the friction velocity, τ is the surface shear applied by the wind, and ρ is the water density. On this basis, we can estimate u^* and τ in the present case to be approximately 1 cm/s and 1 dyne/cm², respectively. The mean surface drift was also approximated by tracking the

downstream displacement of the thermal patterns manually in the clean region near the ridge. Using this procedure, the centerline drift velocity has been determined to be about 2% of the wind speed (see Fig. 3). This result is in reasonable agreement with the result reported by Cheung and Street (1988). The cold region downstream of the

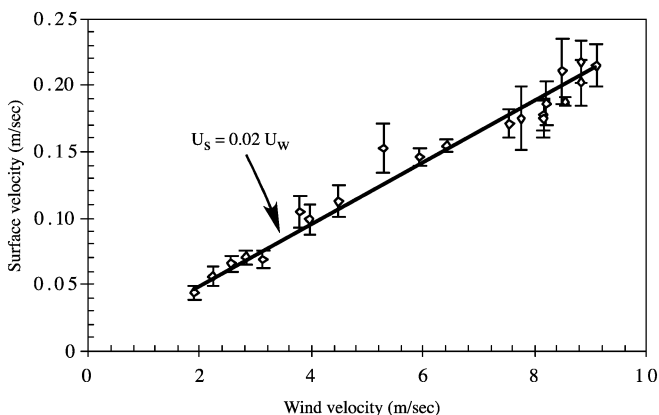


Fig. 3. Plot of the free surface velocity. The surface velocity is calculated from the centerline region of an IR image at different wind speeds. The best fit slope is through all data with the intercept forced through the origin. U_s and U_w are the surface drift velocity and the wind velocity, respectively

Reynolds ridge can be assumed to be the contaminated region. This association of warm and cold regions with clean and contaminated surfaces, respectively, has been recently confirmed in both experiments and numerical simulations (Saylor et al. 2000b; Handler et al. 2003).

Figure 4a displays an IR snapshot of the flow at a time after the Reynolds ridge has reached a time-stationary position. We note that, although the flow is highly turbulent and, therefore, unsteady, it has now reached a statistically steady state. While it is difficult to detect in a still frame, after observing numerous movies of the IR imagery, the advection of hot and cold fluid parcels provides a clear sense of the surface flow pattern. These observations lead to the schematic shown in Fig. 4b, where we have been able to identify three distinct regions of the surface flow. The regions are identified as: (1) the clean (hot) region upstream of the ridge, (2) the cold (contaminated) region downstream, and (3) the wake region. In viewing the time sequences of the imagery, the laminae in the clean region are clearly seen to advect downstream and appear to be subducted beneath the Reynolds ridge. In addition, Fig. 4b shows that the contaminated region contains two areas of recirculation. The recirculation can be interpreted as a return flow caused by the impingement of the main flow onto the sluice. These recirculations appear after the ridge reaches its stationary position. The

central region of each recirculation is primarily made up of warmer fluid surrounded by bands of cooler fluid. The intermediate mixing (wake) region is also evident. We interpret its existence as a result of the mixing of warm fluid from the clean region with cooler fluid from the region of contamination. We notice that the flow appears somewhat asymmetric with respect to the centerline. At this time, we have no clear explanation for this, except to observe that at some lower flow speeds, the asymmetry lessens. Finally, we note that the angle formed by the Reynolds ridge and the side walls of the tank is about 50° , which we find, somewhat surprisingly, to be essentially independent of flow speed in the range 2.5–8.5 m/s.

We have tacitly assumed, as in previous studies (Saylor et al. 2000a; Handler et al. 2001; Saylor et al. 2000b), that the Reynolds ridge coincides with the temperature front, as indicated in Fig. 4a, b. To confirm this conjecture in a rigorous way, we have obtained corresponding IR and visual images of the region of interest. A magnified section of the IR image in the vicinity of the Reynolds ridge (Fig. 4c) is displayed adjacent to the corresponding visual image (Fig. 4d). The right-hand side of these images is 1.9 cm from the channel wall and the top of the image is 10.6 cm from the leading edge of the channel. The surface flow on the downstream side of the ridge is visualized by seeding the surfactant-contaminated layer with silver-

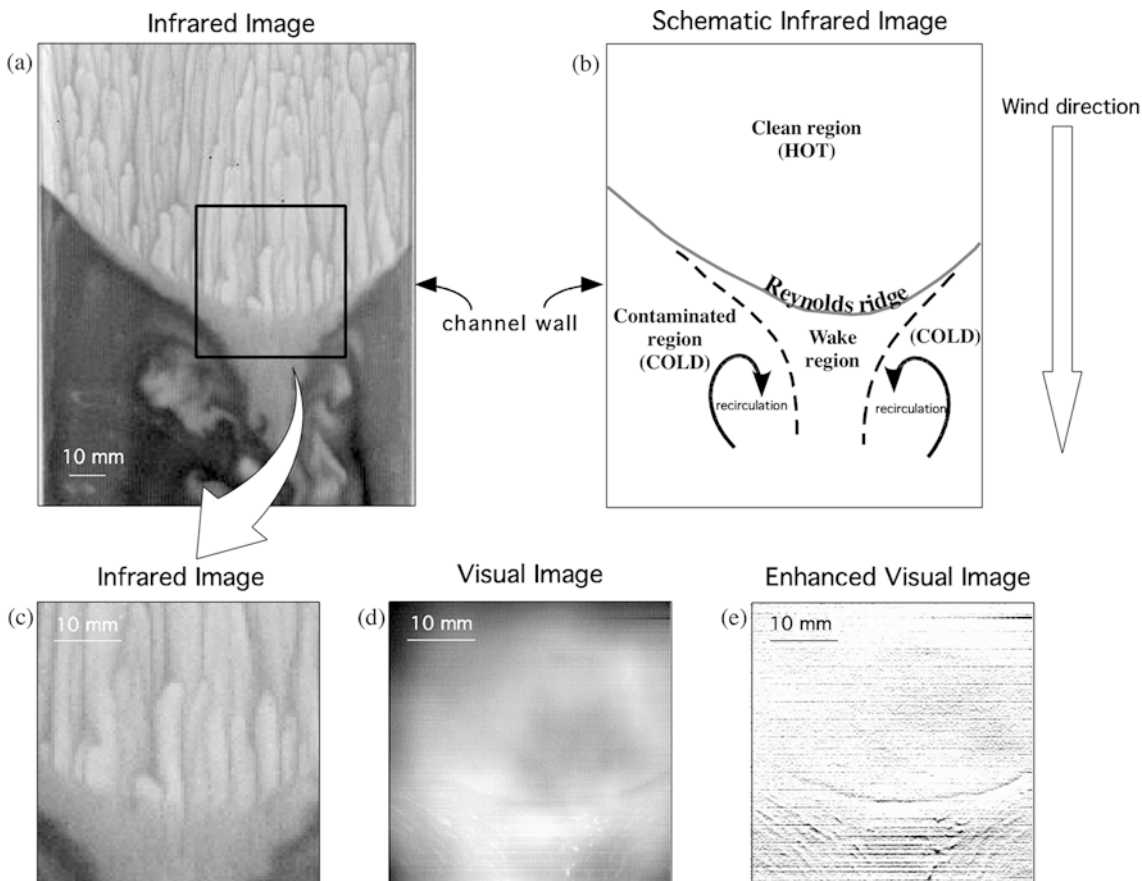


Fig. 4. a IR image of the free surface flow at a wind speed of 7.5 m/s at steady state. The image is 10.4 cm \times 12.8 cm and its top is 6.1 cm downstream from the leading edge of the channel. b Schematic sketch of image a, showing our interpretation of the surface flow and temperature structure near the Reynolds ridge.

Various features are indicated, as described in the text. c Magnified section of the IR image in the vicinity of the Reynolds ridge. The image is 4.2 cm \times 4.2 cm in size. d Snapshot of the same flow obtained from the HS digital camera. e Enhanced visual image obtained by averaging five HS digital visual images

coated polystyrene particles. This technique was used to detect the ridge's location. It is evident that a dark line spans the width of the visual snapshot (Fig. 4d) and is seen more prominently in the enhanced image (Fig. 4e) at precisely the same location as the temperature front in the collocated IR image. The image in Fig. 4e was obtained by averaging five HS digital visual images after applying a 3×3 convolution kernel to obtain local vertical derivatives of the image. The grayscale of the resulting image is then inverted to show the Reynolds ridge demarcation line on the free surface. To the extent that we can associate the visual image of the surface with the location of the surface elevation due to the Reynolds ridge, we believe we can state that the temperature front (i.e., the front associated with the temperature difference between the hot region and the wake region) corresponds precisely to the ridge.

To further elucidate the nature of the temperature field, we display in Fig. 5 an IR image and a line plot of surface temperature data extracted from that image. Figure 5a displays the temperature obtained along a line corresponding to the centerline of Fig. 5b. The line section reveals a general left-to-right increase in temperature. The change in temperature seen near point A is due to the change in temperature associated with the *fishscale* pattern as defined previously. Point B is associated with the location of the front of the ridge. The change in temperature from point B to point C indicates the location of the wake region as described and shown in Fig. 4b.

4 Discussion

We conclude that the upstream and downstream regions of the wind-driven Reynolds ridge, as revealed by high-resolution IR imagery, possess remarkably complex hydrodynamic and thermal phenomena. The existence of wind at the interface creates a cool thermal boundary layer, known as the cool skin (Ewing and McAlister 1960; Saunders 1969; Wick et al. 1996) at the surface of the water column, due to the removal of heat from the water, principally by evaporative cooling. This thin thermal boundary layer is then disrupted by subsurface turbulence, and is modified by the contaminating surfactant, thus, giving rise to the imagery discussed above. The wind-driven Reynolds ridge represents a confluence of shear and surface tension forces combined with air- and water-side turbulence. In addition, we have shown that, although the subtle nature of the ridge, a typical height of less than 0.2 mm (Sellin 1968; Scott 1972), makes it very difficult to detect with the unaided eye, the IR method described here provides an accurate and unambiguous method for locating the ridge.

The preliminary observations reported herein, however, raise a number of issues which will require further investigation. We observe, for example, that at the surface there must be a balance of shear, surface tension, and viscous forces as follows:

$$\tau + \frac{\partial \sigma}{\partial x} = \mu \frac{\partial u}{\partial z} \quad (1)$$

where σ is the surface tension, u is the streamwise velocity at the surface in the water, μ is the viscosity of water, and x

and z are the streamwise (positive pointing upstream, as shown in Fig. 5) and vertical (positive pointing from the water surface into the air) coordinates, respectively. This equation is the simplified version of the equation given in Warncke and Gharib (2000). The viscous term in the original equation was omitted because it has been reported that the surface (shear) viscosity of oleyl alcohol is negligible for the range of the concentrations that was conducted in this study (Vogel and Hirs 2002). In the clean region of the flow, since τ is negative and $\partial \sigma / \partial x$ is nearly zero, we expect that $\partial u / \partial z$ will be negative. On the other hand, in the region of the Reynolds ridge, we expect strong gradients in surface tension, which should cause $\partial \sigma / \partial x$ to be positive. It is, therefore, conceivable, according to the relation above, that the vertical velocity gradient could be reduced to near-zero in the immediate vicinity on the ridge itself.

Additional issues which remain unresolved concern the physics that determine the angle formed by the ridge and

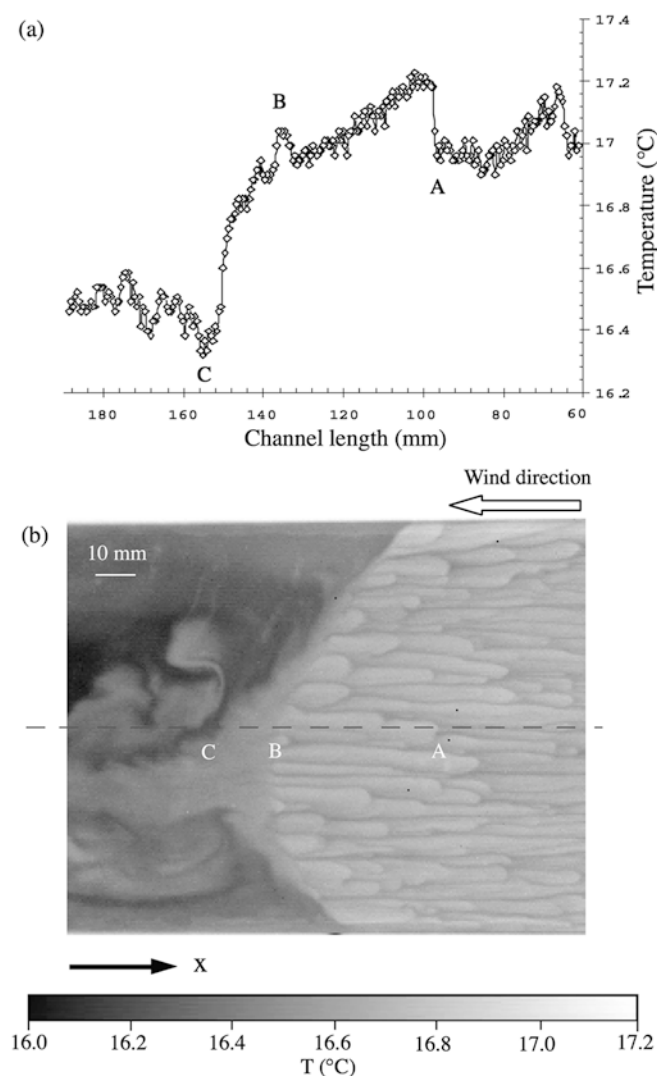


Fig. 5. a A horizontal line section of the temperature through the center of the image presented part b. b An IR image of the free surface flow at a wind speed of 7.5 m/s at steady state (same condition as Fig. 4)

the side walls, the three-dimensional nature of the recirculation zone, and the processes determining the asymmetry mentioned above. Finally, we hope that the results described herein may have some bearing on the dynamics involved in surface slick formation on the ocean surface (Woodcock 1941; Scott 1972; Romano 1996; Saunders 1969; Wick et al. 1996), which are certainly driven in some cases by the wind, and also may assist in the interpretation of the IR signatures in their vicinity.

References

- Cheung TK, Street RL (1988) The turbulent layer in the water at an air-water interface. *J Fluid Mech* 194:133–151
- Edser E (1926) *General physics for students: A text-book on the fundamental properties of matter*. Macmillan, London, pp 636–645
- Ewing G, McAlister ED (1960) On the thermal boundary layer of the ocean. *Science* 131:1374–1376
- Franklin B, Brownrigg W, Farish (1774) Of the stilling of waves by means of oil. Extracted from sundry letters between Franklin, Brownrigg, and the Reverend Mr. Farish. *Philos T* (1683–1775) 64:445–460
- Handler RA, Smith GB, Leighton R (2001) The thermal structure of an air-water interface at low wind speeds. *Tellus* 53A:233–244
- Handler RA, Leighton RI, Smith GB, Nagaosa R (2003) Surfactant effects on passive scalar transport in a fully developed turbulent flow. *Int J Heat Mass Tran* 46:2219–2238
- Harper JF, Dixon JN (1974) In: *Proceedings of the 5th Australasian conference on hydraulics and fluid mechanics*, Christchurch, New Zealand, pp 499–505
- Langmuir I (1938) Surface motion of water induced by wind. *Science* 87:119–123
- Langton J (1872) Ripples and waves. *Nature* 5:241–242
- Leibovich S (1983) The form and dynamics of Langmuir circulations. *Annu Rev Fluid Mech* 15:391–427
- McCutchen CW (1970) Surface films compacted by moving water: Demarcation lines reveal film edges. *Science* 170:61–64
- Reynolds O (1900) Paper on mechanical and physical subjects. Reprinted from various transactions and journals, vol 1. Cambridge University Press, Cambridge, pp 411–412
- Romano JC (1996) Sea-surface slick occurrence in the open sea (Mediterranean, Red Sea, Indian Ocean) in relation to wind speed. *Deep-Sea Res, Part I* 43(4):411–423
- Satterly J, Turnbull R (1929) The ridge at the junction of clean and contaminated liquid surfaces. *T Roy Soc Can* 23:95–118
- Saunders PM (1969) The temperature at the ocean-air interface. *J Atmos Sci* 24:269–273
- Saylor JR, Smith GB, Flack KA (2000a) Infrared imaging of the surface temperature field of water during film spreading. *Phys Fluids* 12:597–602
- Saylor JR, Smith GB, Flack KA (2000b) The effect of a surfactant monolayer on the temperature field of a water surface undergoing evaporation. *Int J Heat Mass Tran* 43:3073–3086
- Scott JC (1972) The influence of surface-active contamination on the initiation of wind waves. *J Fluid Mech* 56(3):591–606
- Scott JC (1982) Flow beneath a stagnant film on water: The Reynolds ridge. *J Fluid Mech* 116:283–296
- Sellin RHJ (1968) Existence of a surface tension discontinuity at a liquid free surface. *Nature* 217:536–538
- Smith GB, Leighton RI, Tang ST (1998) Turbulent transition in the infrared. *Phys Fluids* 10(9):S9–S9
- Veron F, Melville WK (2001) Experiments on the stability and transition of wind-driven water surfaces. *J Fluid Mech* 446:25–65
- Vogel MJ, Hirsra AH, Kelley JS, Korenowski GM (2001) Simultaneous measurement of free-surface velocity and surfactant concentration via a common laser probe. *Rev Sci Instrum* 72(2):1502–1509
- Vogel MJ, Hirsra AH (2002) Concentration measurements downstream of an insoluble monolayer front. *J Fluid Mech* 472:283–305
- Warncke A, Gharib M, Roesgen T (1996) Flow measurements near a Reynolds ridge. *J Fluid Eng-T ASME* 118:621–624
- Warncke A, Gharib M (2000) Experimental study of the wake behind a surface-piercing cylinder for a clean and contaminated free surface. *J Fluid Mech* 402:109–136
- Wick GA, Emery WJ, Kantha LH, Schluskel P (1996) The behavior of the bulk-skin sea surface temperature difference under varying wind speed and heat flux. *J Phys Oceanogr* 26(10):1969–1988
- Woodcock AH (1941) Surface cooling and streaming in shallow fresh and salt water. *J Mar Res* 4(2):153–161